Simulation, characterisation and analysis of Silicon mach zender interferometer.
Literature Review

O.M.Kiely

Compiled: 14 April 2025

Abstract

Silicon is the basis of the majority of electronics and thus is one of the most well-researched materials of the last few decades. Hence, as photonic research progresses, interest in utilising silicon for light applications only increases. Silicon has an indirect band gap and thus is inefficient in generating light. However, due to its large refractive index of 3.45 at 1.55 μm, low cost and electrical properties, silicon photonics is an active area in both industry and research. In this paper, the basic process of simulation, fabrication, experimentation and analysis will be demonstrated using a simple passive device, a Mach Zender interferometer.

---

1 Introduction

Silicon is a ubiquitous material for the well-developed field of electronics. This is because of its affordability, low cost, and electrical properties. In decades of research, silicon fabrication with CMOS techniques has been very well researched, making silicon an ideal material choice for many applications [1]. One application is within photonics. Photonics is the manipulation of light to solve problems such as telecommunication (radio over fibre), metrology (optical combs for atomic clocks) and sensing (LiDAR). Silicon is an indirect bandgap and thus unsuitable for the generation of light; however, with a bandgap of over 1.1eV, silicon is transparent to infrared light and has a high refractive index of 3.45 [1]. Hence, silicon may not be the ideal choice for an active device. Still, it has great potential for passive devices in the telecom range. A typical configuration utilises silicon dioxide (refractive index 1.45) as a substrate for silicon devices, called silicon on insulators (SOI). The refractive index difference of 2 between silicon and silicon dioxide causes strong confinement of light [2]. Due to this, silicon has paved the way for cheap waveguides with more minor bends, including strip waveguides with bends as low as 5μm [2].

This report will discuss the design and fabrication of silicon Mach Zehnder interferometers (MZI) on silicon dioxide as a method of exploring the engineering principles of passive devices and demonstrating the design process. The purpose is to provide an introduction to silicon photonics design. The process will start with 2D mode solver simulations to find parameters for the waveguide. Lumerical interconnect will then be used to find the parameters for the MZIs. Klayout will be used to create the GDS file, which will then be fabricated using Ebeam. The devices will be characterised and analysed.

2 Theory

2.1 Parameters

The refractive index of a material is a measure of the confinement of light, as light will tend toward areas of high refractive index. Thus, a waveguide with a core of 3.44 (silicon) surrounded by a cladding of 1.44 (silicon dioxide) will have a good mode confinement. However, 3.44 is the refractive index of bulk silicon; in our waveguide configuration, a better description of light propagation can be found in the effective index. The effective index measures the phase delay in a material relative to

the phase delay in a vacuum. It changes depending on material, geometry and mode.
Group index is a measure of dispersion and is given by equation 1 [3].

$$n_g = n_{eff} + \lambda(\frac{\delta n_{eff}}{\delta \lambda}) \quad (1)$$

Thus, the rate of change of the effective index will affect the dispersion within the waveguide. So, when choosing mode confinement using width vs effective index, it's advantageous to choose a lower gradient, as it'll make the group index less dependent on fabrication.
A parameter important for resonators and interferometers is the free spectral range (FSR), which is a measure of the distance in frequency space of resonant peaks. Equation 2 describes the free spectral range for an inferemoter with path length difference, ΔL, a group index of n_g at a wavelength, λ.

$$FSR = \frac{\lambda^2}{n_g \Delta L} \quad (2)$$

2.2 Waveguide

In this report, a simple strip waveguide will be explored with the aim of single-mode operation. Thus, dimensional analysis is required to ensure only the fundamental mode propagates[2]. Section 3.1 discusses the geometric considerations for the fabricated waveguides, but sub-micrometres dimensions are usually required [2]. The height of the waveguides in this paper will be fixed by 0.22μm as this is the industry standard thickness of silicon[3]. Polarisation is also controlled via the waveguide dimension. TE has a disadvantage in that the electric component will suffer scattering due to the rough sidewalls caused by etching during fabrication. TM modes scatter from the epitaxially grown top and bottom walls and thus scatter less. Since the height is 0.22μm, the final design is likely to be wider than it is tall, and quasi-TE will be the dominant mode [2]. Thus, within the report, simulations will be made to further confine the devices in the TE configuration. To achieve TE confinement, the width and effective index will be simulated, and a normal width which cuts off the higher order mode will be used [3].
Dimensions also affect the available bend radius of the waveguides. A thin waveguide is less tolerant of a small bend radius due to mode mismatch [3]. In this report, devices will vary by width to explore the effect of width on transmission, loss and performance.
A general description of a waveguide can be found in the compact model of the waveguide. A polynomial formed from a Taylor expansion as in equation 3.

$$n_{eff}(\lambda) = n_1 + n_2(\lambda - \lambda_0) - n_3(\lambda - \lambda_0)^2 \quad (3)$$

This gives us an approximation for the effective index at different wavelengths.
The waveguides for the MZIS are modelled using Lumerical's finite difference eigenmode solver (FDE). FDE solves the eigenmodes for Maxwell's equations [4]. The solver works in 2D and is thus a quick simplifying tool that still yields accurate results.

2.3 Interferometer

The interferometer to be fabricated consists of a waveguide, Y-splitter and grating coupler. The light is injected into the system using the grating couplers. The mode is then passed to a Y-splitter where it's split 50-50 and propagates down two waveguides which form arms. These arms have different lengths and thus lead to constructive or destructive interference when recombined [5]. If we consider an input of intensity,I_i, into a lossless Y-splitter system with a propagation constant of, $\beta = \frac{2\pi n_1}{\lambda}$ where n_1 is found from the compact model of the waveguide, then we can simplify the system into the equation 4 [5].

$$I_0 = \frac{I_i}{2}[1 + \cos(\beta_1 L_1 - \beta_2 L_2)] \quad (4)$$

This equation describes a sinusoidal output dependent on wavelength and optical path length difference in a configuration known as a mismatched interferometer [5]. This can be used to decide on the lengths of the interferometer analytically and estimate experimental results using both equations 4 and 2.

3 Modelling and Simulation

3.1 Strip Waveguide Geometry

The straight silicon waveguide is modelled using Lumerical's mode solver with a fixed height of 0.22μm and an initial thickness of 0.5μm as in figure 1. The simulation area is inside an arbitrarily large SiO2 layer of 4μm by 4μm. The FDE simulation area is within this, with a mesh size of 1000 cells. Running this gives the effective index of the available modes. This report will focus on the first TE mode as shown in figure 2 .

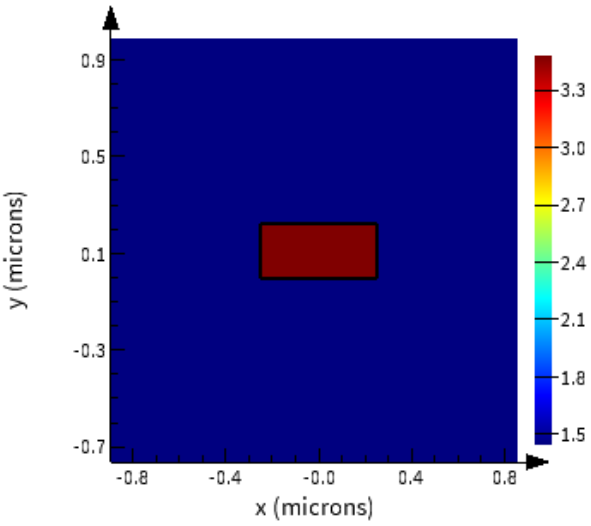

Figure 1: Refractive index profile of SOI waveguide with a height of 0.22μm and a width of 0.5 μm.

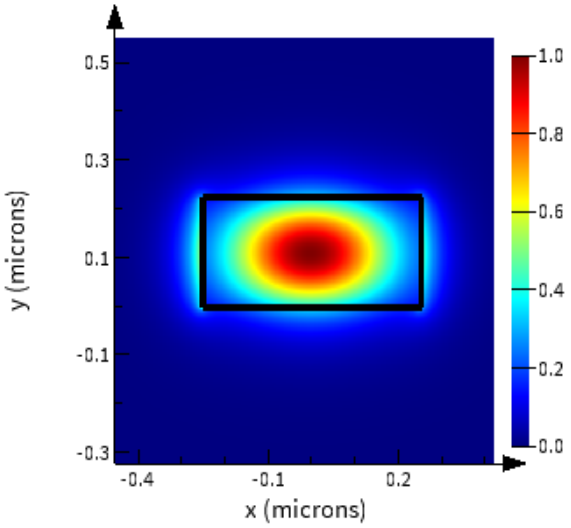

Figure 2: E field intensity of the first mode with an effective index of 2.50.

The final design will vary in width. Thus, a sweep is done of the effective index and base width of the straight waveguide as shown in figure 3.

As the width increases, the index tends toward the refractive index of bulk silicon. It's also noted that below an effective index of 1.45, the mode will leak into the substrate. In the final design, some MZIs will vary by width to see the effect of effective index variation on the MZIs. Other designs will have a fixed width of 0.5 μm, to suppress the higher order modes and limit the gradient of change. A steep gradient will mean slight variations in fabrication have a more significant effect on the refractive index.

To find the waveguide compact model, a sweep is done over wavelength to map the change in the effective index as in figure 4. Polyfitting this yields

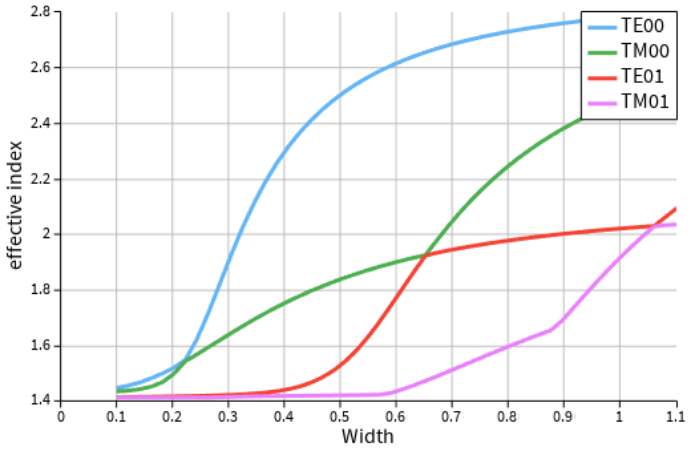

Figure 3: First four modes effective index with width in micrometres. The refractive index of SI02 is 1.45, so anything width below that will cease to function as a waveguide

the waveguide compact model as in equation 5.

$$n_{eff}(\lambda) = 2.45 + 1.15(\lambda - \lambda_0) - 0.45(\lambda - \lambda_0)^2 \quad (5)$$

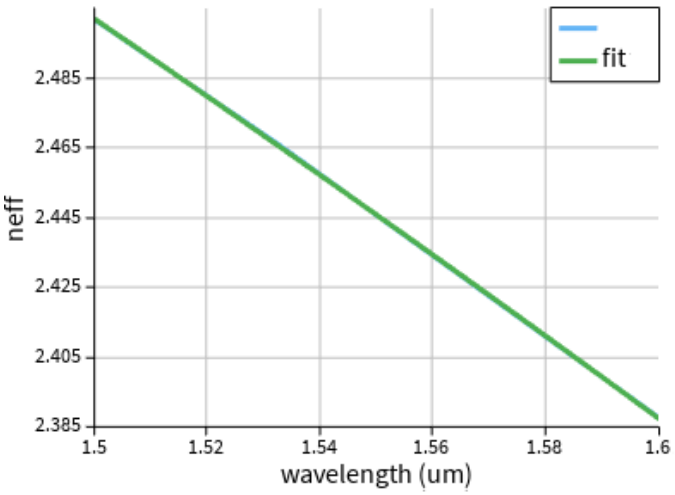

Figure 4: Effective index against wavelength for a-Si strip waveguide with a height of 0.22 μm and width of 0.5 μm.

3.2 Bend Radius

The MZIs require bends, which can lead to loss due to scattering. Firstly, for the standard width of 0.5μm, three modes will be investigated. Then, for every other width, the loss for fundamental TE will be explored. By keeping a low bend, the TE mode will be confined whilst the others will leak. The max radius will be used to limit TE loss. Table 3.2 contains different widths of waveguide with the lowest possible radius whilst still allowing the TE mode to propagate. These different widths will be investigated in the final design.

Width (μm)	bend radi(μm)	Overlap
0.3	7.0	0.996
0.5	2.75	0.995
0.7	2.5	0.968

Table 1: Waveguide variations for final design

3.3 Mach Zhender Interferometer

The interferometer to be fabricated is made of two Y splitters connected by waveguides. Table 2 gives the parameters of the MZI with which the transfer function will be calculated.

Parameter	Value	Reason
λ range(μm)	1.5:1.6	Telecoms
n_1, n_2, n_3	2.45,-1.15,-0.45	WG function
n_{eff} w=0.5	2.50	Standard
Alpha (μ^{-1})	0.001	Simulations
ΔL (μm)	100	Interference

Table 2: Starting parameters for the simulation of the MZI

Using the parameters in table 2, the waveguide loss is calculated for the width of 0.5μm as 0.03 dB/cm. Thus, three different lengths can be explored in some of the designs. The fabricated designs will have different arm lengths to explore the effect on the FSR as described by equation 2. The group index is required to calculate a simulated FSR. The group index is the phase delay in the medium as compared to a vacuum and can be described by equation 6

$$n_g = n_{eff}(\lambda) - \lambda \cdot \frac{dn}{d\lambda} \tag{6}$$

Thus, to calculate the group index, a sweep over wavelength with effective index is undertaken to get the rate of change of effective index with wavelength. From this, the group index and FSR can be found. Table 3 shows the range of FSR values across the telecom range for different arm lengths of the MZIs. Figure 5 demonstrates a typical spectrum for an MZI.

3.4 Corner Analysis

In order to predict the range of expected values due to fabrication difference, corner analysis needs to be used. In this, five simulations are run to find the variation in the expected parameters. An example is displayed in figure 6 and table 5.2 in which

Δ L (μm)	FSR range (nm)
50	13.1 - 14.6
100	5.76-7.15
150	3.85-4.76
200	2.86 - 3.64

Table 3: Different path length differences for exploration in fabricated devices

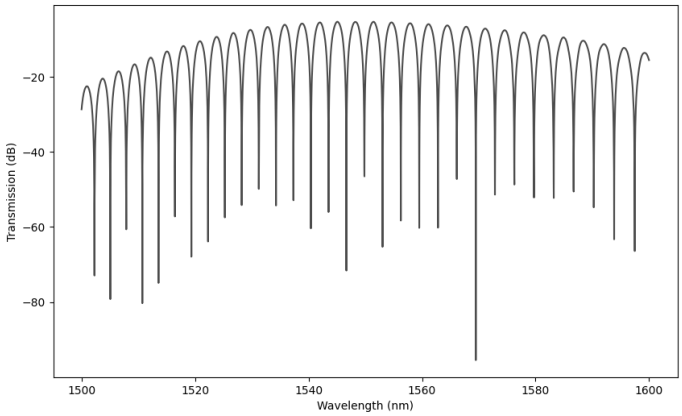

Figure 5: MZI transfer function demonstrating the expected transmission graph (on a linear scale) for an MSI with a width of 0.5μm and an optical path difference of μm 200.

a waveguide of width 500nm and MZI with an optical path length difference of 50μm is used. The extremes of any variation are run for each simulation, giving the highest and lowest values of the group index one can expect.

4 Fabrication

The simulations gave the parameters for different MZIS. To further explore the physics of MZI, a variation of both waveguide width and optical path

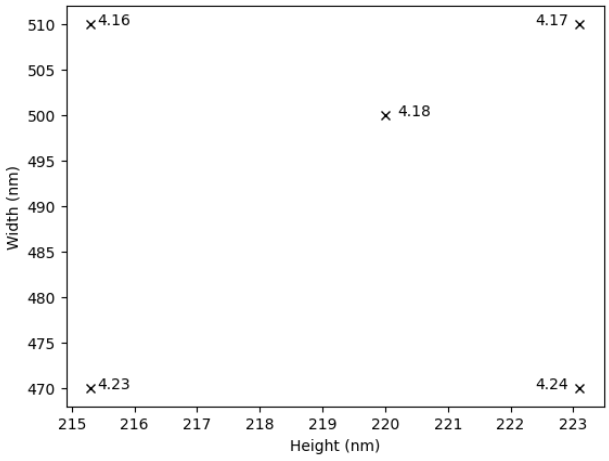

Figure 6: Visual representation of the corner analysis method.

Height (nm)	Width (nm)	n_{eff}	n_g
220	500	2.45	4.18
215.3	470	2.38	4.23
223.1	470	2.41	4.24
215.3	510	2.44	4.16
223.1	510	2.47	4.17

Table 4: Values of simulations run by changing design parameters in Lumerical MODE.

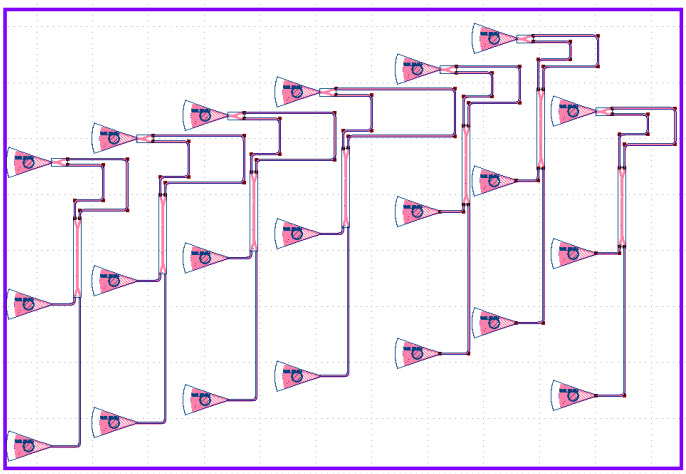

Figure 7: GDS file of silicon MZI's with varying optical path length differences and waveguide thicknesses.

length difference is used. Devices MZI1 and MZI5 are identical to explore the limits of fabrication and the repeatability of the beam.

The devices to be fabricated are thus recorded in table 5.2.

Device name	ΔL (μm)	width (μm)	n_g	FSR (nm)
MZI 1	50	0.5	4.24	11.3
MZI 2	100	0.5	4.24	5.7
MZI 3	150	0.5	4.24	3.7
MZI 4	200	0.5	4.24	2.8
MZI 5	50	0.5	4.24	11.3
MZI 6	50	0.3	4.14	11.6
MZI 7	50	0.7	4.01	12.0

Table 5: Table of devices and desired values at 1.55 (μm)

The GDS is displayed in the figure 7, the MZI are 1-7 as read left to right.

Fabrication accuracy and variation depend on factors such as the beam aperture, exposure dosage and etching timings. Thus, no devices will exactly match the simulations.

4.1 Fabrication

The photonic devices were fabricated using the NanoSOI MPW fabrication process by Applied Nanotools Inc. (http://www.appliednt.com/nanosoi; Edmonton, Canada) which is based on direct-write 100 keV electron beam lithography technology. Silicon-on-insulator wafers of 200 mm diameter, 220 nm device thickness and 2 µm buffer oxide thickness are used as the base material for the fabrication. The wafer was pre-diced into square substrates with dimensions of 25x25 mm, and lines were scribed into the substrate backsides to facilitate easy separation into smaller chips once fabrication was complete. After an initial wafer clean using piranha solution (3:1 H2SO4:H2O2) for 15 minutes and water/IPA rinse, hydrogen silsesquioxane (HSQ) resist was spin-coated onto the substrate and heated to evaporate the solvent. The photonic devices were patterned using a JEOL JBX-8100FS electron beam instrument at The University of British Columbia. The exposure dosage of the design was corrected for proximity effects that result from the backscatter of electrons from exposure of nearby features. Shape writing order was optimised for efficient patterning and minimal beam drift. After the e-beam exposure and subsequent development with a tetramethylammonium sulfate (TMAH) solution, the devices were inspected optically for residues and/or defects. The chips were then mounted on a 4" handle wafer and underwent an anisotropic ICP-RIE etch process using chlorine after qualification of the etch rate. The resist was removed from the surface of the devices using a 10:1 buffer oxide wet etch, and the devices were inspected using a scanning electron microscope (SEM) to verify patterning and etch quality. A 2.2 µm oxide cladding was deposited using a plasma-enhanced chemical vapour deposition (PECVD) process based on tetraethyl orthosilicate (TEOS) at 300ºC. Reflectrometry measurements were performed throughout the process to verify the device layer, buffer oxide and cladding thicknesses before delivery.

5 Experimental Data

5.1 Measurement Method

To characterise the devices, a custom-built automated test setup [3, 6] with automated control software written in Python was used [7]. An Agilent 81600B tunable laser was used as the input source, and Agilent 81635A optical power sensors as the output detectors. The wavelength was swept from

1500 to 1600 nm in 10 pm steps. A polarisation maintaining (PM) fibre was used to maintain the polarisation state of the light, to couple the TE polarisation into the grating couplers [8]. A 90º rotation was used to inject light into the TM grating couplers [8]. A polarisation-maintaining fibre array was used to couple light in/out of the chip [9].

5.2 Results

The experimental data is plotted in figure 8, in which resonance patterns of all seven MZI's can be seen. Table 5.2 shows the experimental group index and FSR.

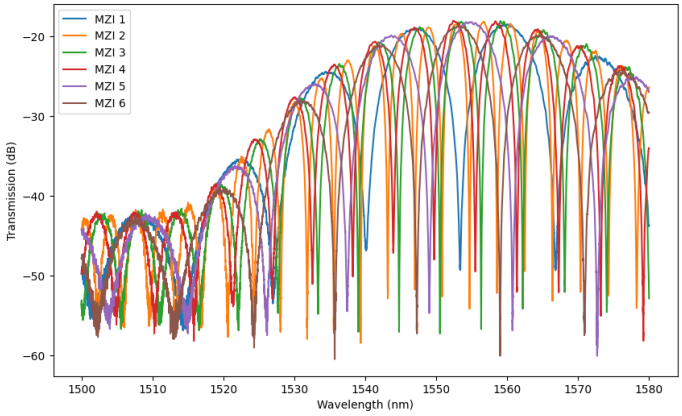

Figure 8: MZI experimental data with the group index and FSR.

The increase in power across the waveguide is due to the wavelength-specific grating responses. The FSR was found using sci-py and then used to calculate the group index using equation 2. The group index, and thus the FSR, is dependant on wavelength, so the values given here are for the peak closest to 1550nm.

Device name	**ΔL (μm)**	**width (μm)**	n_g	FSR (nm)
MZI 1	50	0.5	3.63	13.30
MZI 2	100	0.5	4.16	7.64
MZI 3	150	0.5	4.17	5.77
MZI 4	200	0.5	4.16	5.77
MZI 5	50	0.5	4.14	11.58
MZI 6	50	0.3	4.28	11.23
MZI 7	50	0.7	4.01	12.0

Table 6: Table of devices and desired values at 1.55 (μm)

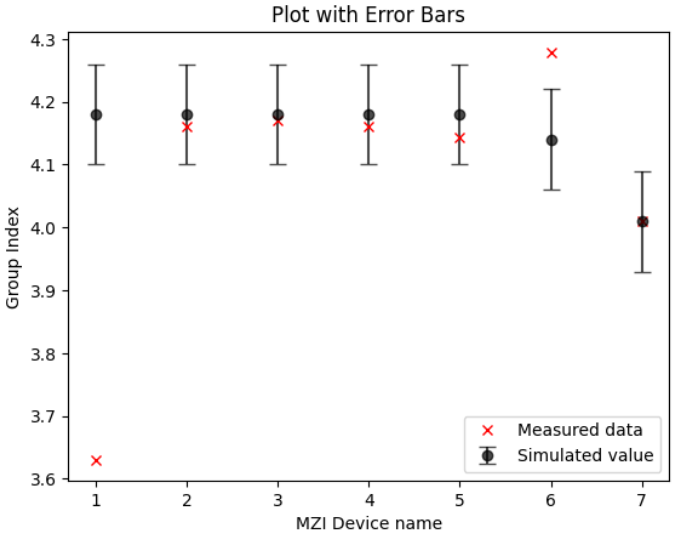

Figure 9: simulated data with error bars and the measured data of the group index.

6 Analysis

The simulated results with errors given by corner analysis are displayed in figure 9 alongside the measured data.

It can be seen that the majority of measured data falls within the acceptable range of values due to fabrication differences. MZI1 is quiet different, with a FSR of 13nm, this implys the arms do not have a difference of 50μm and thus has a different group index. Likewise, MZI6 is outside the range, to understand why SEMs would need to be taken to see how the thin waveguide has effected the spectra.

6.1 Repeatability

Figure 10 demonstrates the spectra of the two rings which were supposed to be identical. However, due to the odd group index, there may be a physical difference that causes the difference in spectra. It is also possible that temperature differences have caused dimension changes during measurement.

7 Conclusion

The devices demonstrate the use of the optical path length difference between two arms can control the FSR. For further investigation, SEMs would be needed to find the reason for the discrepancy in the group index. However, most of the devices fall within the ranges as calculated with the corner analysis.

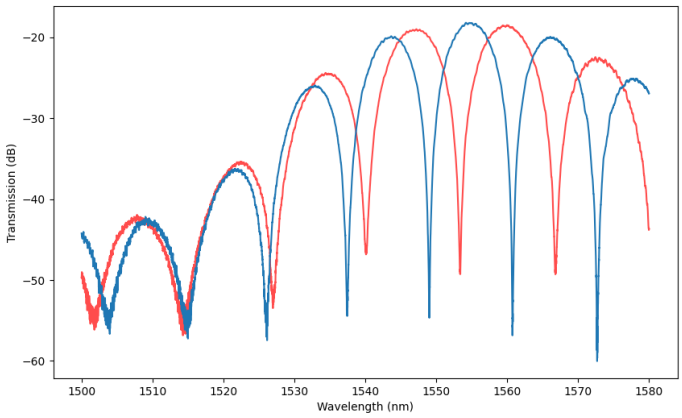

Figure 10: Spectra of two rings with the same specifications. Differences could be due to etches and temperature differences.

8 Acknowledgements

I acknowledge the edX UBCx Phot1x Silicon Photonics Design, Fabrication and Data Analysis course, which is supported by the Natural Sciences and Engineering Research Council of Canada (NSERC) Silicon Electronic-Photonic Integrated Circuits (SiEPIC) Program. The devices were fabricated by Cameron Horvath at Applied Nanotools, Inc. Omid Esmaeeli performed the measurements at The University of British Columbia. We acknowledge Lumerical Solutions, Inc., Mathworks, Mentor Graphics, Python, and KLayout for the design software.

References

[1] B. Jalali and S. Fathpour, "Silicon photonics," *Journal of Lightwave Technology*, vol. 24, no. 12, pp. 4600–4615, 2006.

[2] W. Bogaerts, P. de Heyn, T. van Vaerenbergh, K. de Vos, S. K. Selvaraja, T. Claes, P. Dumon, P. Bienstman, D. van Thourhout, and R. Baets, "Silicon microring resonators," 1 2012.

[3] L. Chrostowski and M. Hochberg, *Optical Materials And Waveguides*, p. 49–91. Cambridge University Press, 2015.

[4] L. Chrostowski and M. Hochberg, *Modelling And Design Approaches*, p. 28–46. Cambridge University Press, 2015.

[5] L. Chrostowski and M. Hochberg, *Fundamental Building Blocks*, pp. 92–161. Cambridge University Press, 4 2015.

[6] "http://mapleleafphotonics.com," *Maple Leaf Photonics.*, Seattle WA, USA.

[7] M. Caverley, "http://siepic.ubc.ca/probestation,"

[8] Y. Wang *et al.*, "Focusing sub-wavelength grating couplers with low back reflections for rapid prototyping of silicon photonic circuits,"

[9] P. Connections, "www.plcconnections.com," *Columbus OH, USA*.